The Electrical Characteristics of the Conical Horn-Reflector Antenna

By J. N. HINES, TINGYE LI and R. H. TURRIN

(Manuscript received February 11, 1963)

The conical horn-reflector antenna was selected for the satellite communication ground station because of its broadband and low-noise properties. Prior to the construction of the full-size antenna, theoretical and model studies of its electrical characteristics were undertaken. These studies consisted of computing gain and radiation patterns for two modes of excitation, constructing of model antennas and measuring them. Results of these studies are presented in this paper together with results of the measurements of the full size antenna at Andover, Maine.

I. INTRODUCTION

The horn-reflector antenna was selected for the satellite communication ground station because of its broadband and low-noise properties along with certain operational advantages. Two forms of the horn-reflector antenna exist, the pyramidal and the conical. The *pyramidal* horn-reflector antenna has been widely used in the Bell System's microwave radio relay network since its inception at Bell Telephone Laboratories, Holmdel, New Jersey, over 20 years ago.[1] Recently, a large steerable version of this antenna with a 20 × 20-foot aperture[2] was built at Holmdel, New Jersey, and employed in both the Echo and Telstar communications satellite projects. More recently, a very large *conical* horn-reflector antenna was constructed at Andover, Maine, and an identical one at Pleumeur-Bodou, France, for the Telstar communications satellite project. Electrically, the two types of the horn-reflector antenna are very similar, but the conical form possesses certain structural advantages. The suitability and the performance of these antennas are amply reflected in the success of these projects.

Prior to construction of the full-size conical horn-reflector antenna, theoretical and model studies of the electrical characteristics of the antenna were undertaken. These studies consisted of computing gain

and radiation patterns for two modes of excitation, constructing model antennas and measuring them. We present in this paper results of these studies together with results of the measurements of the full-size antenna at Andover, Maine.

II. DESCRIPTION OF ANTENNAS

2.1 *General*

The geometry of the horn reflector is shown in Fig. 1. The antenna consists of a paraboloidal reflecting section illuminated by a conical horn. The apex of the horn coincides with the focus of the paraboloid,

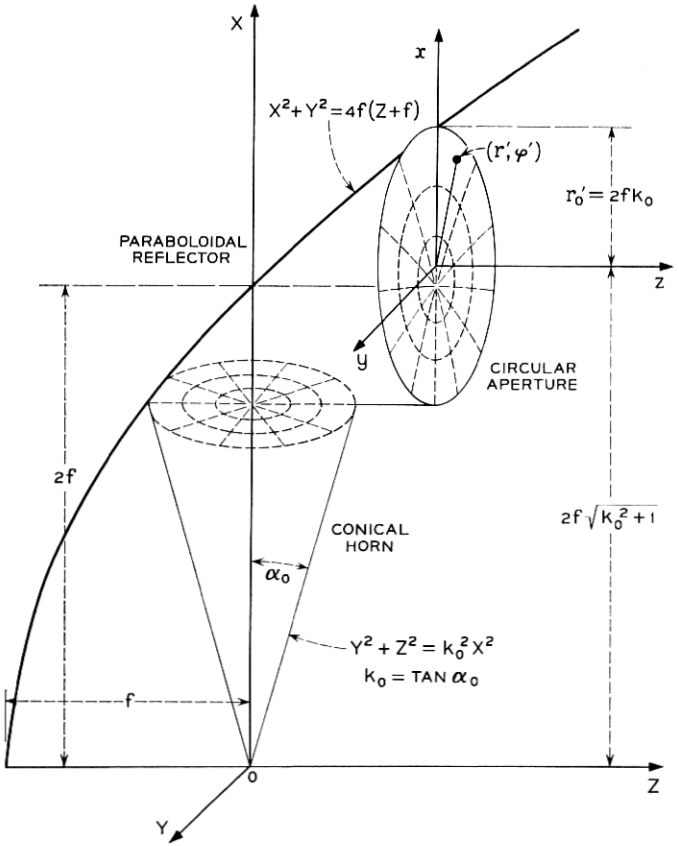

Fig. 1 — Geometry of the conical horn-reflector antenna.

and the axis of the horn is perpendicular to the axis of the paraboloid. The paraboloidal section acts as a combined right-angle reflector and phase corrector for the diverging spherical wave from the conical horn, so that the wave appearing at the circular aperture has a plane wavefront. A cylindrical section encircles the aperture and is attached to both the conical horn and the paraboloidal reflector. This cylindrical aperture shield contributes to the low-noise characteristic of this type of antenna.

The antenna can be excited in as many ways as there are modes in the conical horn.[3,4] For small flare angles the field configurations over the spherical equiphase surfaces are essentially the same as those of a circular waveguide. It is certainly true in this case, where the total flare angle is 31.5 degrees. Therefore, we refer to the dominant wave in the horn as the TE_{11} wave and the second propagating wave as the TM_{01} wave. The former is used for communication and the two are used together for automatic tracking.

2.2 *Model Antennas*

Two models of the conical horn-reflector antenna were constructed at the Holmdel and at the Whippany, N. J., Bell Laboratories. These are referred to as models one and two, respectively. Photographs of these model antennas are shown in Fig. 2. Model one was employed for extensive TE_{11} mode pattern measurements, while model two was employed primarily to investigate the TM_{01} mode radiation patterns. Neither model was measured to exact scale of the large antenna (in terms of wavelength). Pertinent dimensions and information about the models are given in Table I.

The reflector surface of model one was constructed of $\frac{1}{16}$-inch brass strips which form sectors of the paraboloid. The strips, approximately two inches wide, were bonded to a rigid ribbed frame with a resin cement. The surface accuracy was obtained with the aid of precision templates; the surface was then hand honed. The reflector surface of model two was constructed with the aid of a paraboloidal deep dish which was used as a mold. The dish surface tolerance, therefore, determined the tolerance of the reflector of the model antenna. Both models had aperture shields which were cut in a plane tangent to the cone surface.

2.3 *Full Size Antenna*

A sketch of the full-size antenna constructed at Andover, Maine, is shown in Fig. 3. The mechanical design of the antenna is reported else-

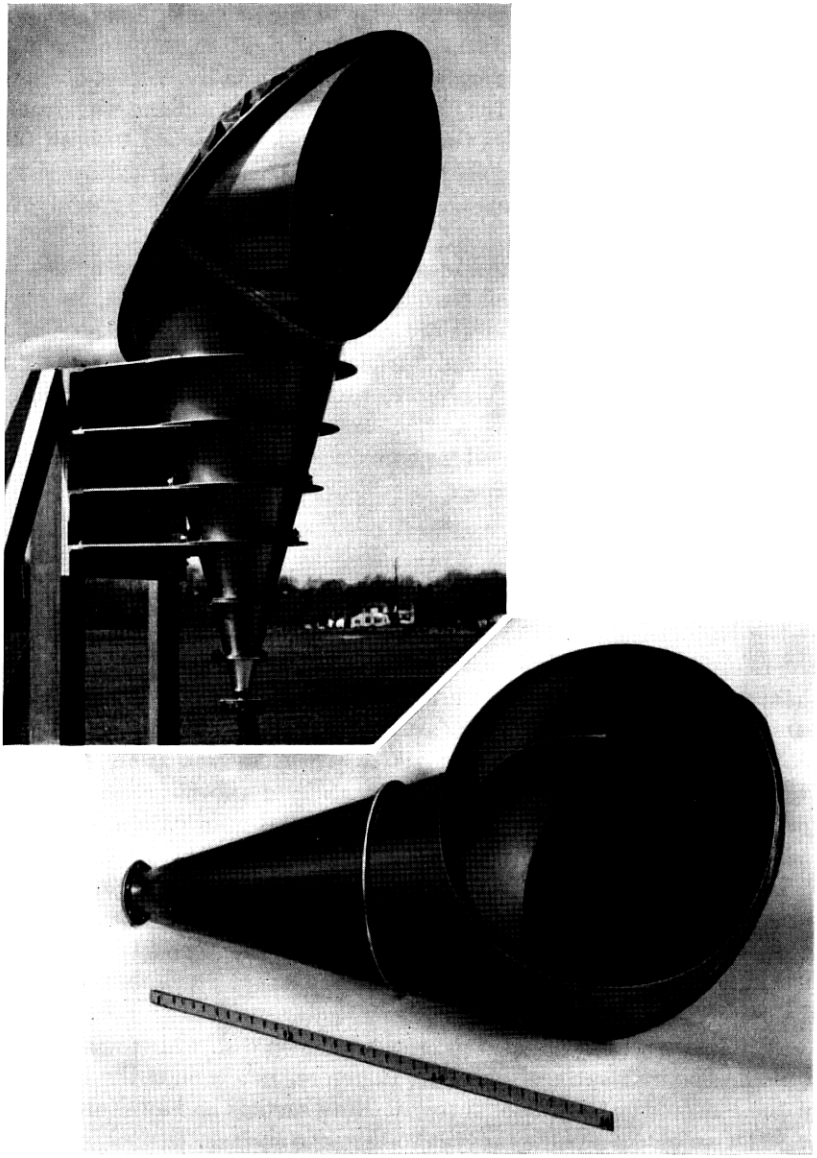

Fig. 2 — Photographs of the model antennas: upper, model one; lower, model two.

TABLE I

	Model One	Model Two
Aperture diameter	27 inches	23 inches
Flare angle	31.5 degrees	27 degrees
Measuring frequency	11.2 kmc	10.0 kmc
Construction material	Brass sheet	Resin-impregnated Fiberglas coated with silver paint
Reflector surface tolerance	±0.010 inch	±0.060 inch

where.[5] Some of the important features of the antenna are given in Table II.

The antenna and support structure rotate about a central pintle bearing on two sets of tracks for azimuth motion. Elevation motion is accomplished by rotating the antenna about its cone axis. A rotary joint is located in the cone section approximately 6 feet from the apex. The entire antenna structure is enclosed in a 210-foot diameter radome.

III. THEORETICAL PATTERN COMPUTATION

The paraboloidal section of the antenna transforms the spherical wave in the conical horn into a plane wave. However, due to the curvature of the reflector and the differences of path length involved, the aperture field configuration is not the same as that in the horn but is somewhat distorted; the field lines tend to crowd toward that edge of the aperture closest to the apex of the horn. The amount of distortion depends upon the flare angle of the horn and becomes more pronounced as the angle increases.

Equations relating coordinates in the cone with coordinates in the aperture plane are derived in Appendix A. In essence, polar coordinates in the cone are transformed into bipolar coordinates in the aperture plane (see Fig. 1). The transformation is therefore conformal.

Once the equations of transformation are known, the linear (x and y) components of the aperture fields for the TE_{11} wave and the TM_{01} wave can be written; these are given in Appendix B. Since the principal electric vector of the TE_{11} wave can be arbitrarily oriented in the aperture plane, we have chosen two principal directions of polarization for our computation. One of these is designated longitudinal polarization, where the principal electric vector in the aperture plane is parallel to the axis of the cone; the other is designated transverse polarization, where the principal electric vector in the aperture plane is orthogonal to the axis

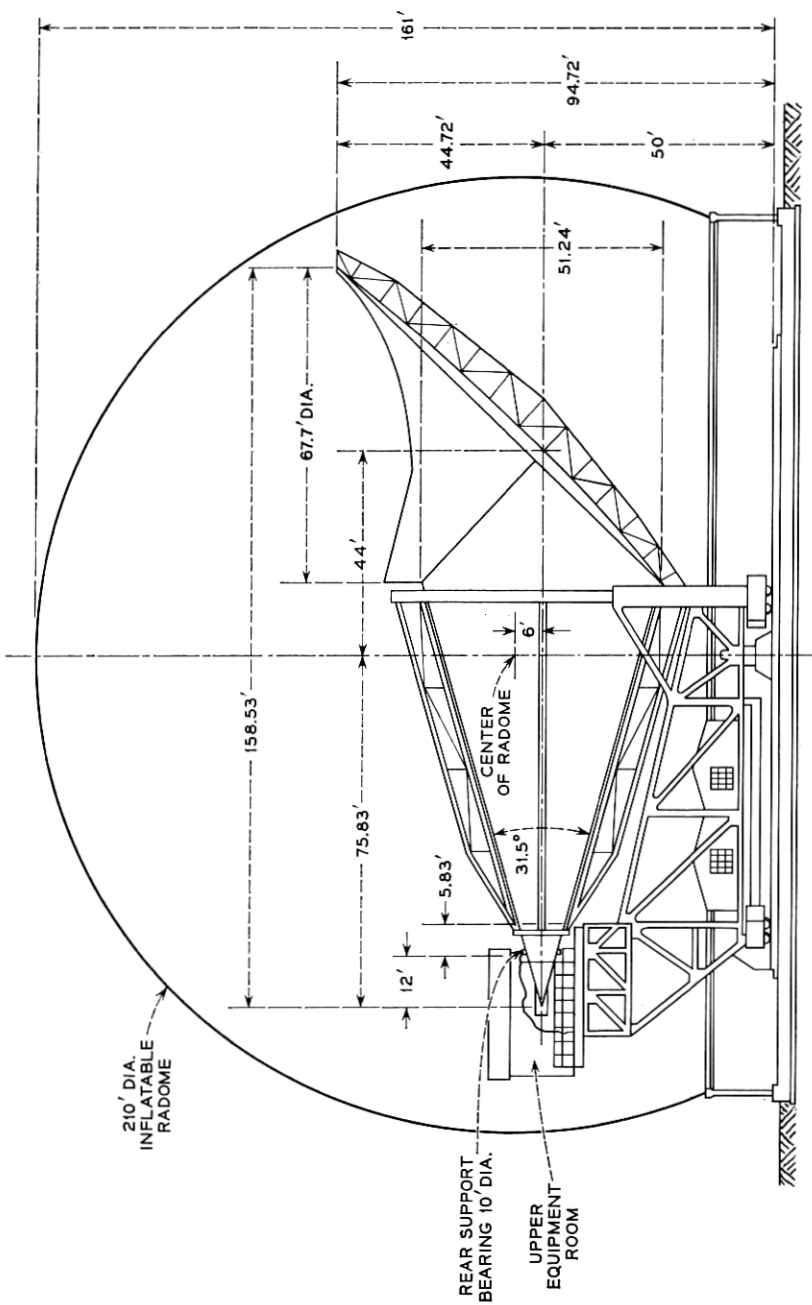

Fig. 3 — Sketch of the full-size conical horn-reflector antenna at Andover, Maine.

TABLE II

Total flare angle of conical horn	31.5 degrees
Focal length of paraboloid	60 feet
Diameter of aperture	67.7 feet = 280 wavelengths at the receiving frequency of 4079.73 mc and 440 wavelengths at the transmitting frequency of 6389.58 mc.
Aperture area	3600 square feet

of the cone. The TM_{01} wave, however, is axially symmetric in the conical horn and therefore has no principal direction of polarization.

The aperture fields being known, one can calculate the far-field patterns of the antenna near the axis of the beam to good approximation by using the integral[6]

$$g(\theta,\varphi) = \frac{1}{4f^2}\int_0^{2\pi}\int_0^{r_0'} E(r',\varphi')\exp[j\beta r'\sin\theta\cos(\varphi-\varphi')]r'\,dr'\,d\varphi' = \int_0^{2\pi}\int_0^{k_0} E(s,\varphi')\exp[jus\cos(\varphi-\varphi')]s\,ds\,d\varphi' \tag{1}$$

where $E(r',\varphi')$ represents the components of the aperture field under consideration, $\beta = 2\pi/\lambda$ is the propagation constant of free space, f is the focal length of the paraboloid, $k_0 = \tan\alpha_0 = \tan(\frac{1}{2}$ flare angle of the cone), $r_0' = 2f\,k_0$ is the radius of the aperture, and $u = 2\beta f\sin\theta$. As illustrated in Fig. 1, the polar coordinates $r'(s = r'/2f)$ and φ' are in the aperture plane, and the angles θ and φ refer to the polar (z) axis through the center of the aperture plane.

We have computed the radiation patterns in two principal (longitudinal and transverse) planes and in a 45-degree plane. The longitudinal plane contains the beam and the horn axes; the transverse plane contains the beam axis but is normal to the horn axis (see Fig. 4). Since the aperture fields are symmetric about the longitudinal plane, the integral given by (1) can be reduced further. The reduced integrals for the various cases are listed in Appendix C. These integrals were programmed for numerical integration on an IBM 704 computer.

The computed patterns of the antenna excited by a TE_{11} wave are given in Figs. 5, 6 and 7, which show (as dashed curves) the principal and the cross-polarized patterns for longitudinal and transverse polarizations and in the two principal planes. Because the cross-polarized components of the aperture fields are antisymmetric about the longitudinal plane, the cross-polarized patterns for both polarizations are zero for all angles in that plane and therefore are not shown. Fig. 8 gives the

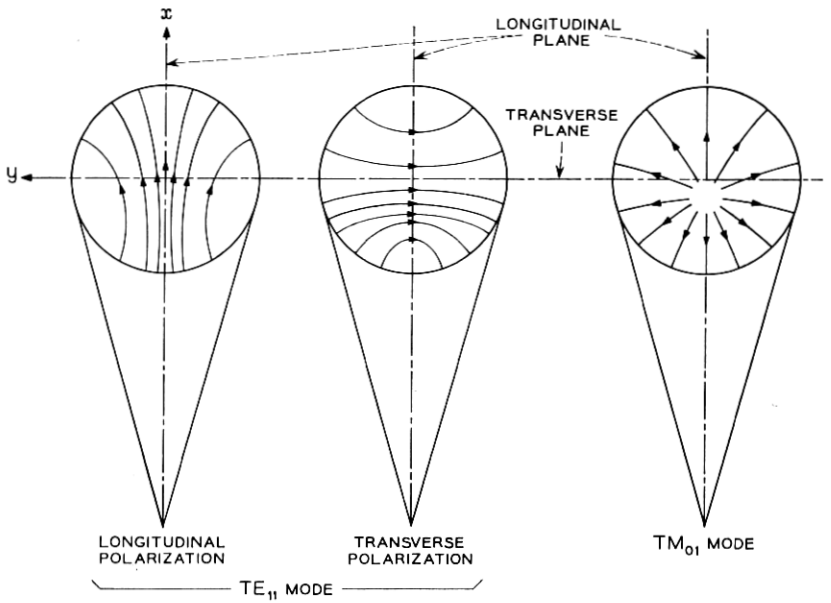

Fig. 4 — Sketch showing the electric field lines in the aperture plane of the antenna for the two modes of excitation. The principal planes in which radiation patterns are calculated and measured are also indicated.

computed radiation patterns of the antenna excited by a TM_{01} wave. Fig. 8(a) shows the pattern in the longitudinal plane for the longitudinal component of the field, and Fig. 8(b) shows the pattern in the transverse plane for the transverse component of the field. The pattern for the transverse component is zero for all angles in the longitudinal plane, and all the lobes of the pattern for the longitudinal component are more than 50 db down in the transverse plane; these patterns therefore are not shown.

The aperture efficiencies of the antenna excited by a TE_{11} wave are calculated to be 0.806 for the longitudinal polarization and 0.807 for the transverse polarization.

The radiation patterns for circular polarization may be calculated by combining the appropriate principal and cross-polarized components of the far field.[2] The computed patterns in the longitudinal and in the transverse planes are shown in Figs. 9 and 10. Due to the presence of the cross-polarized components of the far field in the transverse plane, the circularly polarized radiation patterns in the transverse plane are unsymmetrical; the maximum of the main beam is shifted by 0.97 u off the $u = 0$ axis, which is about one-thirteenth of the 3-db beamwidth. The

direction of this shift is dependent upon the sense of the polarization, the shift being $+0.97\ u$ for one sense and $-0.97\ u$ for the other.

Certain salient features of the antenna are summarized in Table III for linear polarization and in Table IV for circular polarization. For example, at the receiver frequency of 4170 mc the power gain and the half-power beamwidth for circular polarization are 58.17 db and 0.228°, respectively, and at the transmitter frequency of 6390 mc they are 61.86 db and 0.149°, respectively.

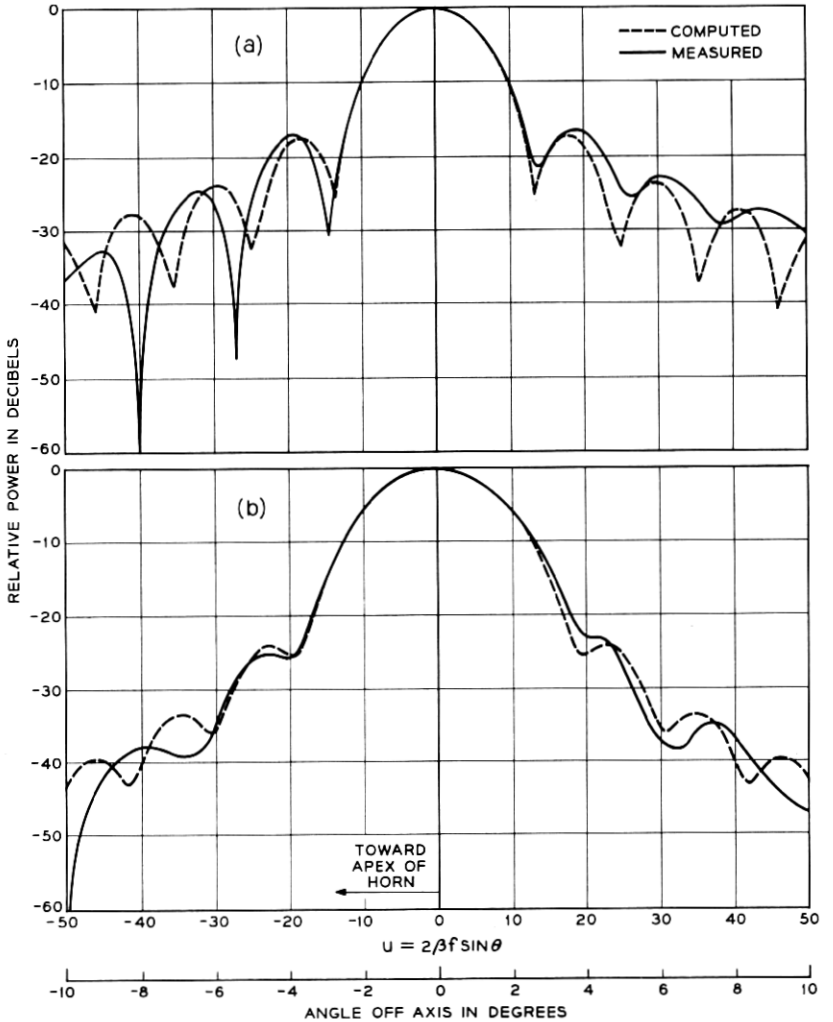

Fig. 5 — Radiation patterns for TE_{11} mode in the longitudinal plane (model one): (a) longitudinal polarization; (b) transverse polarization.

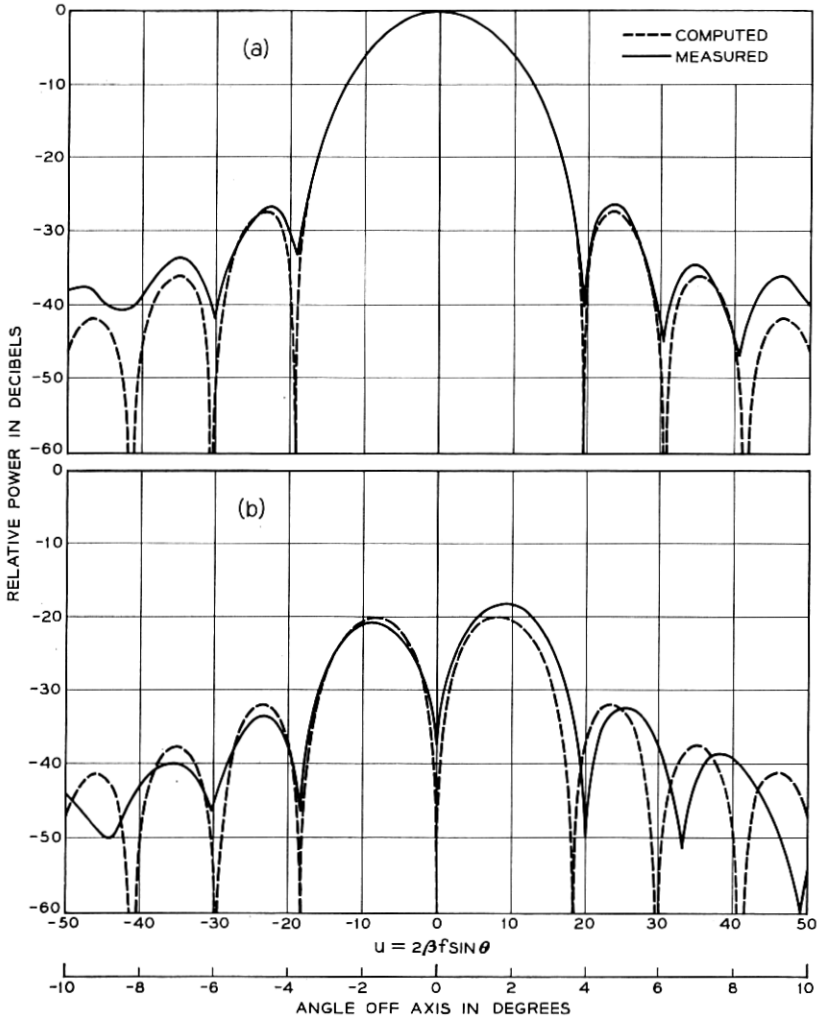

Fig. 6 — Radiation patterns for TE_{11} mode in the transverse plane (model one): (a) principal patterns for longitudinal polarization; (b) cross-polarized patterns for longitudinal polarization.

IV. MEASURED RESULTS

4.1 *Model Antennas*

Far-field radiation pattern measurements for linear polarization were made on both model antennas and showed good agreement with theoretically computed patterns. Both antennas were measured on outdoor

ranges where standard antenna measuring procedure was employed. In particular, TE_{11} mode patterns for both longitudinal and transverse polarizations were measured on model one at 11.2 kmc. The measured patterns in longitudinal and transverse planes are shown as solid curves along with the computed patterns in Figs. 5 through 7. The TM_{01} mode patterns which were important to automatic tracking were measured

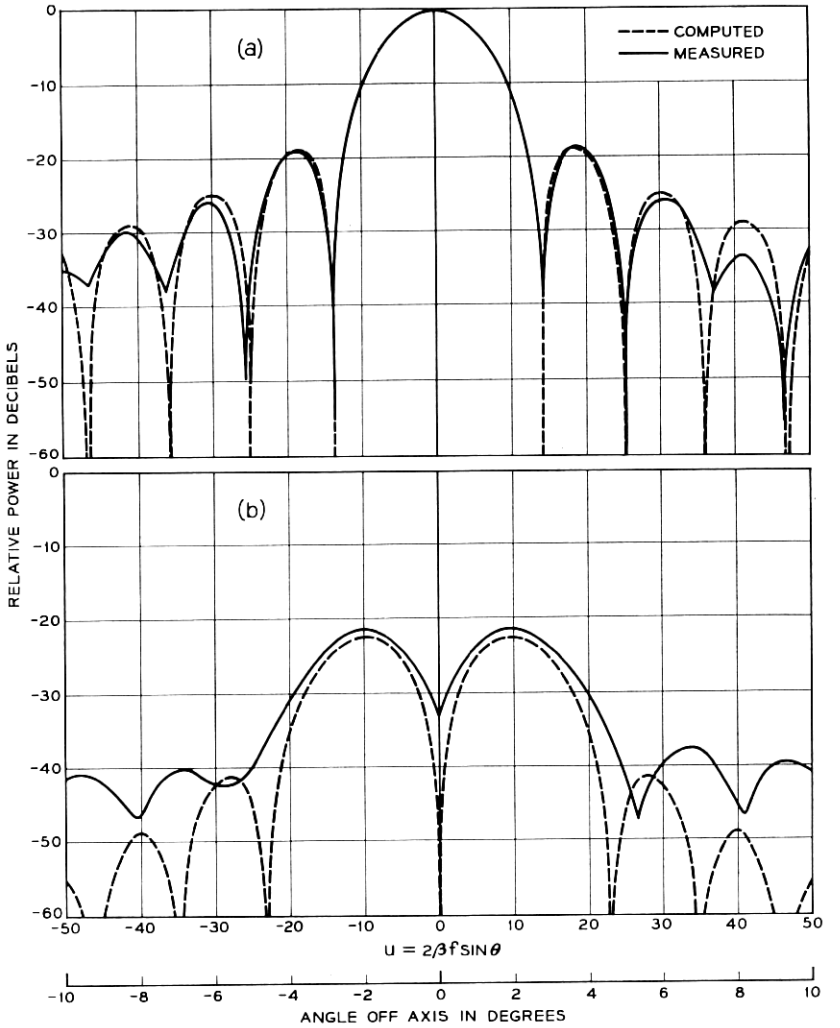

Fig. 7 — Radiation patterns for TE_{11} mode in the transverse plane (model one): (a) principal patterns for transverse polarization; (b) cross-polarized patterns for transverse polarization.

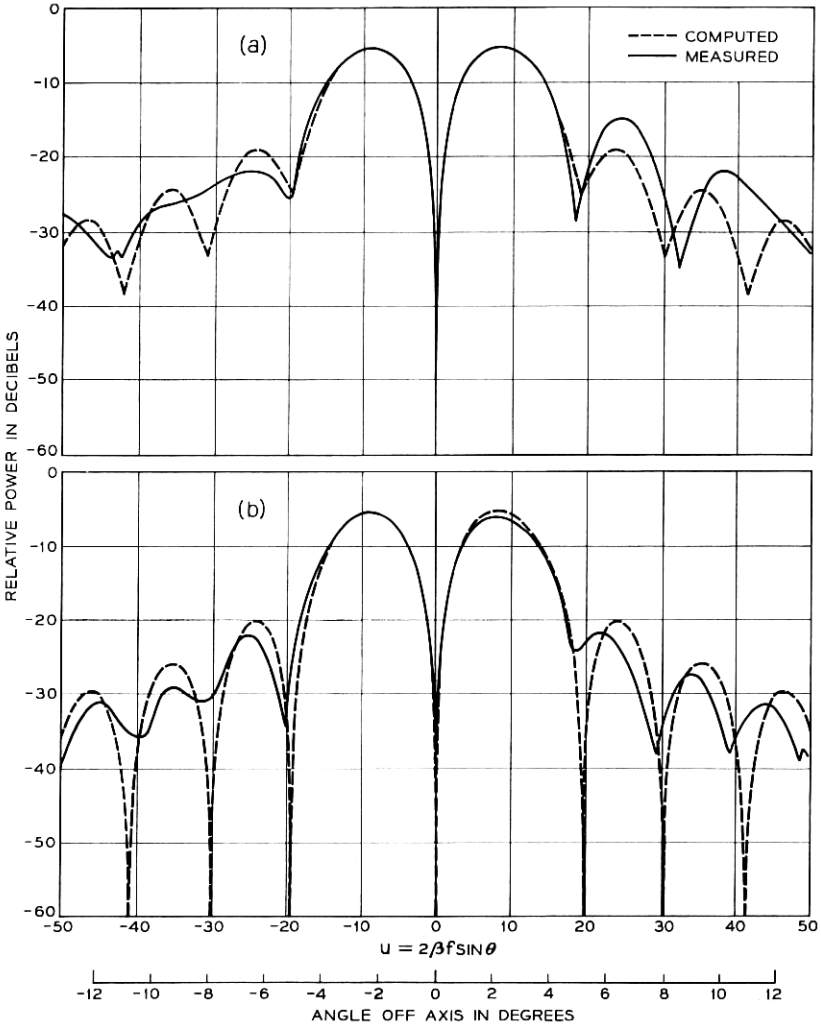

Fig. 8 — Radiation patterns for TM_{01} mode (model two): (a) in the longitudinal plane for the longitudinal component of the aperture field; (b) in the transverse plane for the transverse component of the aperture field.

on model two; these patterns are characterized by nulls in the direction of the TE_{11} beam maxima. The measured and computed patterns for the longitudinal component in the longitudinal plane and for the transverse component in the transverse plane are shown in Fig. 8, where the relative power scales are normalized to the TE_{11} mode beam maxima.

In general, the agreement between measured and computed patterns is good, especially in the region of the main beam and first side lobes. The agreement becomes poor for levels near and below the isotropic level. The discrepancies are probably due to a variety of factors which include higher-order modes, depolarization due to ground roughness, mechanical inaccuracies, and approximations involved in the theoretical analysis.

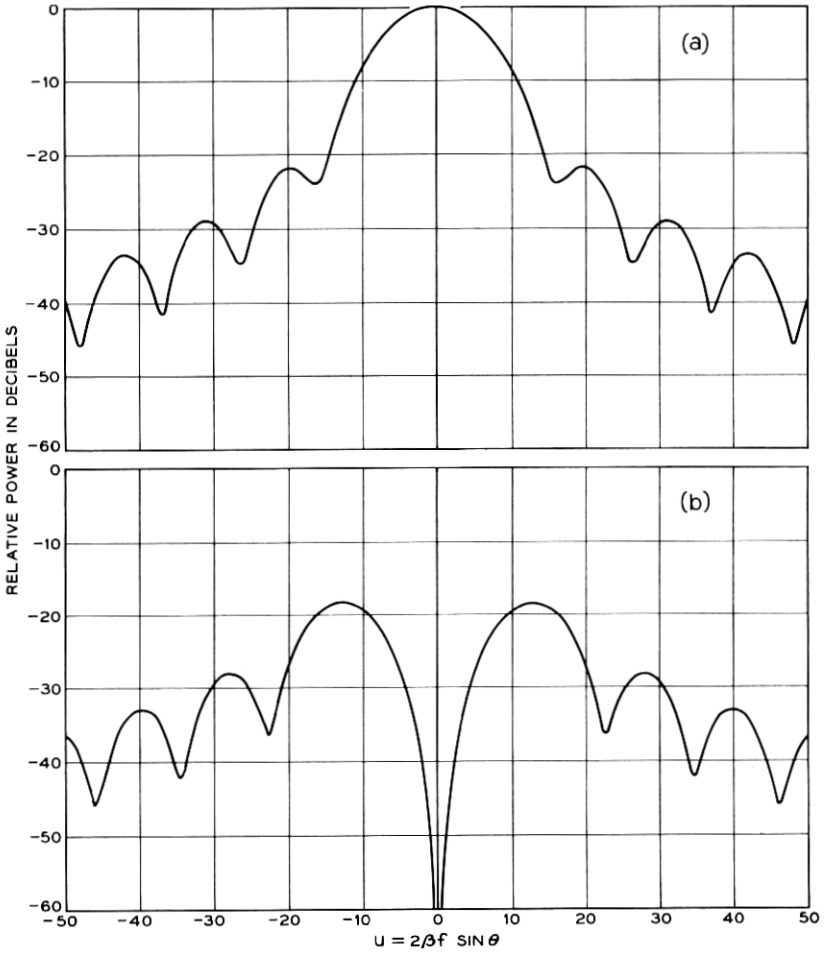

Fig. 9 — Computed circularly polarized radiation patterns for TE_{11} mode in the longitudinal plane: (a) desired sense; (b) undesired sense.

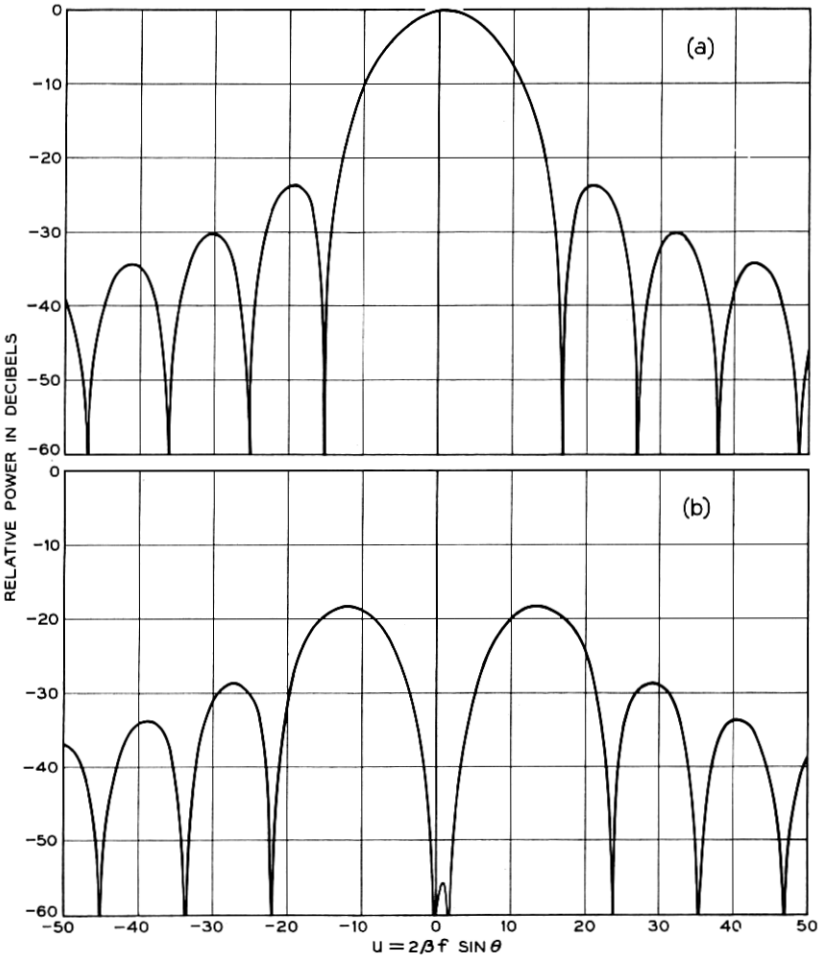

Fig. 10 — Computed circularly polarized radiation patterns for TE_{11} mode in the transverse plane: (a) desired sense; (b) undesired sense.

Gain measurements for both longitudinal and transverse polarization were made on model one, and the difference in gain between the two polarizations was less than the measurement error. The average of the measured gain corresponded to an effective area 1.3 ± 0.2 db less than the actual area. Theoretically the effective area should be 0.94 db less than the actual area.

A characteristic of the horn-reflector antenna is the spillover lobe in

TABLE III — COMPUTED RADIATION CHARACTERISTICS OF THE CONICAL HORN-REFLECTOR ANTENNA FOR LINEAR POLARIZATION (FLARE ANGLE = 31.5°)

TE_{11} Mode	Longitudinal Polarization			Transverse Polarization		
	Long. Plane	Trans. Plane	45° Plane	Long. Plane	Trans. Plane	45° Plane
3-db beamwidth ($u = 2\beta f \sin\theta$)	11.2	14.6	12.7	14.0	11.7	12.7
Null beamwidth ($u = 2\beta f \sin\theta$)	27.2	38.4	32.6	39.0	27.4	32.6
Maximum cross-polarization (db)	$-\infty$	−20.0	−17.7	$-\infty$	−22.3	−17.5
First side-lobe level (db)	−17.2	−27.0	−22.1	−24.1	−18.2	−23.1
2nd side-lobe level (db)	−23.5	−35.8	−29.6	−33.4	−24.5	−29.6
3rd side-lobe level (db)	−27.5	−41.8	−34.1	−39.4	−28.5	−33.6
TM_{01} Mode	Longitudinal Component			Transverse Component		
	Long. Plane	Trans. Plane	45° Plane	Long. Plane	Trans. Plane	45° Plane
Principal-lobe level* (db)	−5.5	−52.7	−8.5	$-\infty$	−5.7	−8.7
Null level* (db)	−52.7		−52.7		$-\infty$	$-\infty$
Width between principal lobes ($u = 2\beta f \sin\theta$)	17.0		17.0		17.0	17.0
Null width at 20 db below peak of principal lobe ($u = 2\beta f \sin\theta$)	1.1		1.1		1.1	1.1
First side-lobe level* (db)	−19.0		−22.6		−20.5	−22.9

* Relative to major-lobe level of TE_{11} mode.

the longitudinal plane with longitudinal polarization caused by diffraction over the edge of the reflector.[2] This spillover lobe in the radiation pattern was measured on model one and found to be at +68° with a level of −35 db from the main beam. The spillover does not occur for transverse polarization because of the taper in the aperture field.

TABLE IV — COMPUTED RADIATION CHARACTERISTICS OF THE CONICAL HORN-REFLECTOR ANTENNA FOR CIRCULAR POLARIZATION (FLARE ANGLE = 31.5°)

TE_{11} Mode	Longitudinal Plane	Transverse Plane
3-db beamwidth ($u = 2\beta f \sin\theta$)	12.7	12.8
Null beamwidth ($u = 2\beta f \sin\theta$)	33.6	32.4
Beam shift ($u = 2\beta f \sin\theta$)	0	0.97
Maximum level of undesired sense of polarization (db)	−18.3	−18.2
First side-lobe level (db)	−21.7	−23.6
2nd side-lobe level (db)	−28.9	−30.1
3rd side-lobe level (db)	−33.3	−34.3

4.2 *Full-Size Antenna*

4.2.1 *General*

A series of measurements and tests were conducted during February, March, and April, 1962, on the antenna at Andover, Maine. These consisted of boresight, gain, polarization and pattern measurements.

The boresight antenna,* located atop a 250-foot tower on Black Mountain 4.6 miles away, was used to illuminate the horn reflector during these measurements. The beamwidth of the boresight antenna and its height above ground were selected so that the maximum level of the ground reflected signal received by the horn reflector would be 45 db or more below the maximum direct signal when the horn reflector is on boresight. Actual measurements indicated that the reflected signal was more than 50 db below the direct signal. Evidence that the incident field was quite uniform in the azimuth plane was obtained when a comparison was made between patterns measured in the normal and plunged positions (i.e., both azimuth and elevation reversed from normal position). The comparison revealed that the two sets are nearly identical; that is, the patterns "turned over" with the antenna.

4.2.2 *Boresighting*

The electrical boresight axis is defined as the direction of the null in the center of the TM_{01} pattern used in the autotrack system. As the initial step in the calibration of antenna pointing, this axis was located and the angle data readouts were set to the boresight antenna coordinates.

The distance to the boresight antenna is approximately 24,000 feet, which is about 37 per cent shorter than that required for the conventional phase deviation of $\pi/8$ radian across the aperture. The effect of boresighting at a reduced range was investigated theoretically.[7] It was found that at this range the null in the TM_{01} pattern shifts in azimuth 0.007 degree away from the aperture normal toward the apex of the horn feed section.

By using a technique of plunging the antenna first in azimuth and then in elevation so as to again point at the boresight antenna, it is possible to determine the precise electrical pointing direction of the antenna with respect to the rotational axes. This was done, and the results of the tests

* The boresight antenna is a two-foot diameter paraboloidal reflector illuminated by a circularly polarized feed. It has a power gain of 25 db and an axial ratio of less than 2 db at 4080 mc.

can be summarized as follows. The magnitude of the parallax with respect to the azimuth axis obtained from the geometry of the ground station is 0.106 degree (the aperture is offset from the axis of azimuthal rotation). Boresighting at the reduced range decreases this angle by 0.007 degree so that the magnitude of the electric azimuth parallax should be 0.099 degree. However, the average measured electrical parallax was 0.123 ± 0.005 degree. This indicates that there is a slight outward pitch of the reflector surface which is equal to one-half this amount, or 0.012 degree, when the antenna is pointing at the boresight tower. The surveyed elevation angle to the boresight tower is 3.960 degrees and the average electrical elevation angle measured by plunging was 3.990 ± 0.005 degrees. The difference indicated an 0.030 ± 0.005 degree droop of the reflector at low elevation. These, along with more recent star-tracking measurements, generally corroborate the sag predicted by structural analysis.

4.2.3 *Gain Measurements*

Because time was at a premium, the usual technique of measuring the vertical distribution of the incident field with the standard gain horn to determine its average value was not employed in measuring the power gain of the horn-reflector antenna. Instead the standard horn was placed at a convenient point at the edge of the roof of the upper equipment room (see Fig. 3). The measured value of power gain was 57.8 ± 0.3 db. To lend support to this measurement, the directivity of the horn reflector was determined by integrating its measured radiation patterns. The value so obtained is 57.6 ± 0.2 db. These results are to be compared with the theoretical value of 57.97 db. The measurements were made at a frequency of 4080 mc.

4.2.4 *Radiation Pattern Measurements*

Radiation pattern measurements were made for the TE_{11} mode and the TM_{01} mode at 4080 mc with the antenna in the position in which it is normally operated. The horizontal and vertical components of the circularly polarized TE_{11} field excited in the circular feed section at the apex of the conical horn were measured. The patterns are called the $(TE_{11})_X$ and $(TE_{11})_Y$ patterns respectively, because they are measured at the horn apex, which does not rotate in elevation with the rest of the antenna. For small changes in elevation about this position, however, $(TE_{11})_X$ essentially corresponds to longitudinal polarization, and $(TE_{11})_Y$ to transverse polarization (see Fig. 4). The TM_{01} patterns were measured

in the same manner. All of these measurements were repeated with the antenna in the plunged position. The normal position patterns are shown and compared with the computed patterns in Figs. 11 to 13. The dashed curves in the figures represent computed patterns of the far field for linear polarization with the exception of the one in Fig. 13(a), which represents the computed pattern in the longitudinal plane at the reduced range.[7]

Agreement between measured and predicted patterns over the sector of the major lobes is excellent and is fairly good in the side-lobe regions. Some discrepancy is to be expected in the side-lobe regions, however, since the measured patterns include the effect of the cross-polarized response of the antenna (the incident field was circularly polarized) while the computed points include only the linearly polarized response of the antenna. In addition, the patterns were measured at a reduced range.

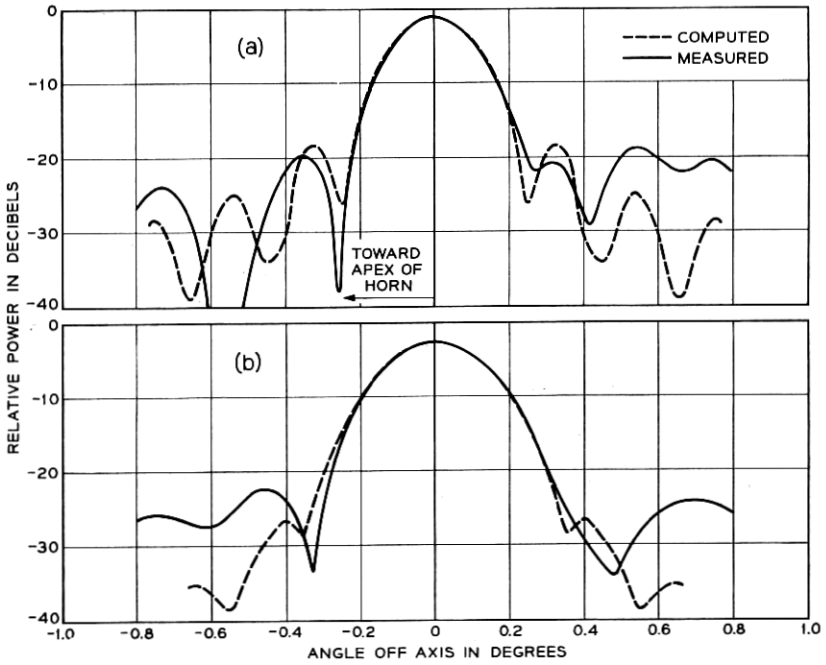

Fig. 11 — Principal radiation patterns of the full size antenna for TE_{11} mode in the longitudinal plane: (a) longitudinal polarization $(TE_{11})_X$; (b) transverse polarization $(TE_{11})_Y$. (The dashed curves are computed far-field patterns.)

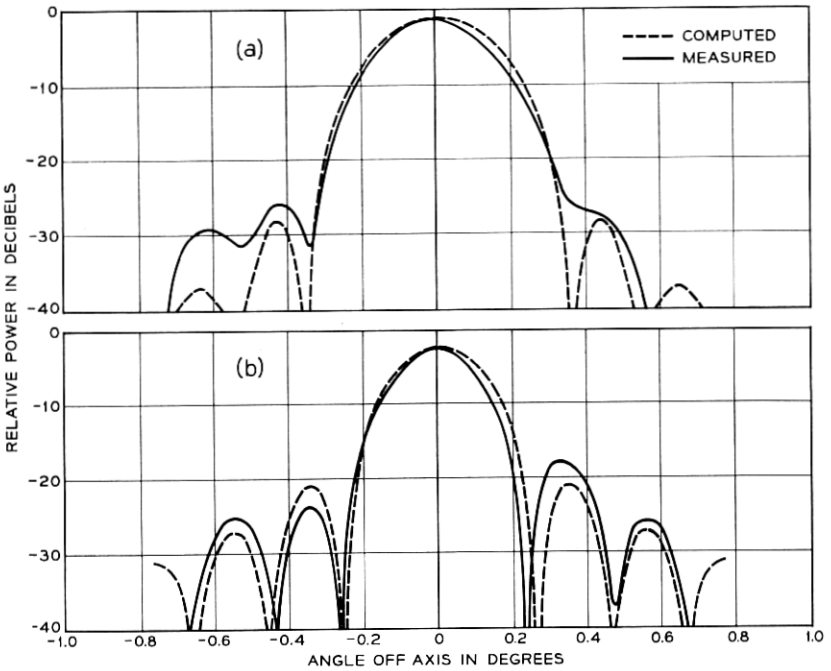

Fig. 12 — Principal radiation patterns of the full size antenna for TE_{11} mode in the transverse plane: (a) longitudinal polarization $(TE_{11})_X$; (b) transverse polarization $(TE_{11})_Y$. (The dashed curves are computed far-field patterns.)

The patterns described above were measured through a construction shelter before the permanent radome was installed. A comparison with those measured later through the permanent radome disclosed no measurable change in the patterns.

V. ACKNOWLEDGMENTS

It is a pleasure to acknowledge the efforts of R. R. Redington for assistance in the construction and adjustment of the boresight antenna and in the measurements on the full-size horn-reflector antenna. E. M. Elam, J. H. Hammond and E. C. Snyder also assisted in the various measurements. Mrs. C. L. Beattie programmed the computer for the pattern and gain computations. The aid and encouragement of A. B. Crawford, J. S. Cook and R. Lowell in these efforts are also acknowledged. In addition, the patience of the people in the servo-control group

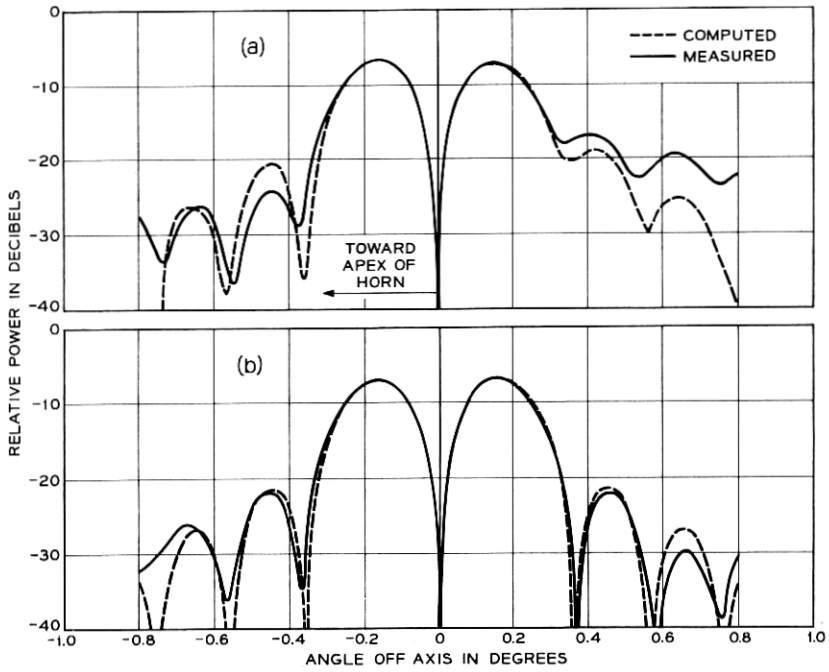

Fig. 13 — Radiation patterns of the full size antenna for TM_{01} mode: (a) in the longitudinal plane for the longitudinal component of the aperture field (the dashed curve is computed for the reduced range); (b) in the transverse plane for the transverse component of the aperture field (the dashed curve is the computed far-field pattern).

and their care exercised in moving the antenna during measurements are greatly appreciated.

APPENDIX A

The Geometry of the Antenna

The geometry of the conical horn-reflector antenna is given in Fig. 1. The apex of the conical section, which is also the focus of the paraboloidal section, is taken to be the origin of the coordinate system (X, Y, Z), and the axis of the cone is taken to be coincident with the X axis.

The equation of a cone coaxial with the conical horn is

$$Y^2 + Z^2 = k^2X^2, \tag{2}$$

where $k = \tan \alpha$ and 2α = flare angle of the cone. The equation of the paraboloid is

$$X^2 + Y^2 = 4f(Z + f), \tag{3}$$

where f is the focal length. Eliminating Z between (2) and (3) gives the equation for the projection of intersection of cone and paraboloid in the X-Y plane. This equation is

$$(X - 2f\sqrt{k^2 + 1})^2 + Y^2 = 4f^2k^2, \tag{4}$$

which is a circle with center at $(2f\sqrt{k^2 + 1}, 0)$ and radius equal to $2fk$. Since (2) also represents circles in the Y-Z plane, we see that the paraboloidal reflector transforms a family of concentric circles in the Y-Z plane into a family of nonconcentric circles in the X-Y plane. Similarly, we can show that a family of radial lines in the Y-Z plane, after reflection from the paraboloid, transforms into a family of circles in the X-Y plane which are described by

$$X^2 + (Y - 2f \cot \eta)^2 = 4f^2 \operatorname{cosec}^2 \eta, \tag{5}$$

where $\eta = \arctan (Y/Z)$ = constant defines the family of radial lines in the Y-Z plane. Equations (4) and (5) describe a set of orthogonal coordinate systems in the X-Y plane. This is the familiar bipolar coordinate system.[8] Therefore, the transformation from the set of polar coordinates in the Y-Z plane into the set of bipolar coordinates in the X-Y plane is a conformal transformation.

APPENDIX B

The Aperture Field

The radial and the circular components of the field in the conical horn are given by

$$E_\rho = \frac{1}{\kappa\rho} J_1(\kappa\rho) \cos \eta \tag{6}$$

$$E_\eta = -\tfrac{1}{2}[J_0(\kappa\rho) - J_2(\kappa\rho)] \sin \eta \tag{7}$$

for TE_{11} mode, longitudinal polarization,

$$E_\rho = \frac{1}{\kappa\rho} J_1(\kappa\rho) \sin \eta \tag{8}$$

$$E_\eta = \tfrac{1}{2}[J_0(\kappa\rho) - J_2(\kappa\rho)] \cos \eta \tag{9}$$

for TE_{11} mode, transverse polarization, and

$$E_\rho = J_1(\gamma\rho) \tag{10}$$

$$E_\eta = 0 \tag{11}$$

for TM_{01} mode. In the above equations $\rho^2 = X^2 + Z^2$, $\tan \eta = Y/Z$ and J_n is a Bessel function of the first kind and nth order. The arguments of the Bessel function $\kappa\rho$ and $\gamma\rho$ are equal to 1.841184 (k/k_0) and 2.404826 (k/k_0), respectively, where $k_0 = \tan \alpha_0$ and $2\alpha_0$ is the total flare angle of the horn.

After reflection from the paraboloidal section, these polar components of the field transform conformally into the corresponding bipolar components in the aperture plane. E_η will lie along the family of circles given by (4) and E_ρ will lie along the orthogonal family of circles given by (5). Since the bipolar coordinate system is a curvilinear system, it is necessary to obtain the linear components of the field before radiation patterns can be computed.

For the purpose of computing radiation patterns, it is convenient to take the center of the aperture as the origin of the coordinate system. Now, the periphery of the aperture is a circle given by (4) with k replaced by k_0. Letting the center of the circular aperture be the origin of a new coordinate system in which

$$x = X - 2f\sqrt{k_0^2 + 1} \quad \text{and} \quad y = Y,$$

equation (4) becomes

$$(x + 2f\sqrt{k_0^2 + 1} - 2f\sqrt{k^2 + 1})^2 + y^2 = 4f^2k^2. \tag{12}$$

This equation gives the direction of E_η in the aperture plane. The angle, ψ_η, which E_η makes with the x axis is given by

$$\tan \psi_\eta = \frac{dy}{dx} = -(x + 2f\sqrt{k_0^2 + 1} - 2f\sqrt{k^2 + 1})/y. \tag{13}$$

Since E_ρ is perpendicular to E_η, the angle ψ_ρ between E_ρ and the x axis is given by

$$\tan \psi_\rho = -\left(\frac{dy}{dx}\right)^{-1} = -\cot \psi_\eta. \tag{14}$$

Knowing the angles ψ_η and ψ_ρ, we can now write expressions for the linear components of the aperture field; they are:

$$E_x = \frac{2f}{d}[E_\rho \cos \psi_\rho + E_\eta \cos \psi_\eta] \tag{15}$$

and

$$E_y = \frac{2f}{d}\left[E_\rho \sin \psi_\rho + E_\eta \sin \psi_\eta\right]. \tag{16}$$

where $d = f + (X^2 + Y^2)/4f$ is the distance from the apex of the horn to the reflector. The factor $2f/d$, therefore, takes into account the attenuation due to path-length difference for the spherical wave in the conical section of the antenna.

APPENDIX C

List of Integrals Used in Pattern Computation

C.1 TE_{11} Mode

(*i*) Longitudinal plane ($\varphi = 0°$ and $180°$)

(a) Principal patterns

$$\begin{matrix} g_L(u) \\ \\ g_T(u) \end{matrix} = \int_0^{\pi} \int_0^{k_0} \begin{matrix} {}_{\mathrm{L}}E_x(s,\varphi') \\ \\ {}_{\mathrm{T}}E_y(s,\varphi') \end{matrix} \exp\left(jus\cos\varphi'\right) s\, ds\, d\varphi'$$

(b) Cross-polarized patterns

$$\begin{matrix} g_L(u) \\ \\ g_T(u) \end{matrix} = 0$$

(*ii*) Transverse plane ($\varphi = 90°$ and $270°$)

(a) Principal patterns

$$\begin{matrix} g_L(u) \\ \\ g_T(u) \end{matrix} = \int_0^{\pi} \int_0^{k_0} \begin{matrix} {}_{\mathrm{L}}E_x(s,\varphi') \\ \\ {}_{\mathrm{T}}E_y(s,\varphi') \end{matrix} \cos\left(us\sin\varphi'\right) s\, ds\, d\varphi'$$

(b) Cross-polarized patterns

$$\begin{matrix} g_L(u) \\ \\ g_T(u) \end{matrix} = \int_0^{\pi} \int_0^{k_0} \begin{matrix} {}_{\mathrm{L}}E_y(s,\varphi') \\ \\ {}_{\mathrm{T}}E_x(s,\varphi') \end{matrix} \sin\left(us\sin\varphi'\right) s\, ds\, d\varphi'$$

(*iii*) 45° plane ($\varphi = 45°$ and 225°)

(a) Principal patterns

$$\begin{matrix} g_L(u) \\ g_T(u) \end{matrix} = \int_0^{\pi} \int_0^{k_0} \begin{matrix} {}_LE_x(s,\varphi') \\ {}_TE_y(s,\varphi') \end{matrix} \cos\left(\frac{us}{\sqrt{2}} \sin\varphi'\right) \exp\left(j\frac{us}{\sqrt{2}} \cos\varphi'\right) s\, ds\, d\varphi'$$

(b) Cross-polarized patterns

$$\begin{matrix} g_L(u) \\ g_T(u) \end{matrix} = \int_0^{\pi} \int_0^{k_0} \begin{matrix} {}_LE_y(s,\varphi') \\ {}_TE_x(s,\varphi') \end{matrix} \sin\left(\frac{us}{\sqrt{2}} \sin\varphi'\right) \exp\left(j\frac{us}{\sqrt{2}} \cos\varphi'\right) s\, ds\, d\varphi'$$

In the above equations the subscripts L and T denote longitudinal and transverse polarizations, respectively.

C.2 TM_{01} *Mode*

(*i*) Longitudinal plane ($\varphi = 0°$ and 180°)

(a) Longitudinal component pattern

$$g_{TM}(u) = \int_0^{\pi} \int_0^{k_0} E_x(s,\varphi') \exp(jus \cos\varphi') s\, ds\, d\varphi'$$

(b) Transverse component pattern

$$g_{TM}(u) = 0$$

(*ii*) Transverse plane ($\varphi = 90°$ and 270°)

(a) Longitudinal component pattern

$$g_{TM}(u) = \int_0^{\pi} \int_0^{k_0} E_x(s,\varphi') \cos(us \sin\varphi') s\, ds\, d\varphi'$$

(b) Transverse component pattern

$$g_{TM}(u) = \int_0^{\pi} \int_0^{k_0} E_y(s,\varphi') \sin(us \sin\varphi') s\, ds\, d\varphi'$$

(*iii*) 45° plane ($\varphi = 45°$ and 225°)

(a) Longitudinal component pattern

$$g_{TM}(u) = \int_0^{\pi} \int_0^{k_0} E_x(s,\varphi') \cos\left(\frac{us}{\sqrt{2}} \sin\varphi'\right) \exp\left(j\frac{us}{\sqrt{2}} \cos\varphi'\right) s\, ds\, d\varphi'.$$

(b) Transverse component pattern

$$g_{TM}(u) = \int_0^{\pi} \int_0^{k_0} E_y(s,\varphi') \sin\left(\frac{us}{\sqrt{2}} \sin \varphi'\right) \exp\left(j \frac{us}{\sqrt{2}} \cos \varphi'\right) s \, ds \, d\varphi'.$$

REFERENCES

1. Friis, H. T., and Beck, A. C., U. S. Patent 2,236,393, filed March 1, 1939, issued March 25, 1941.
2. Crawford, A. B., Hogg, D. C., and Hunt, L. E., A Horn-Reflector Antenna for Space Communication, B.S.T.J., **40,** July, 1961, pp. 1095–1116.
3. Buchholz, H., The Propagation of Electromagnetic Waves in a Conical Horn, Ann. d. Physik, **37,** February, 1940, pp. 173–225.
4. Schorr, M. G. and Beck, F. J., Jr., Electromagnetic Field of the Conical Horn, J. Appl. Phys., **21,** August, 1950, pp. 795–801.
5. Dolling, J. C., Blackmore, R. W., Kindermann, W. J., and Woodard, K. B., The Mechanical Design of the Conical Horn-Reflector Antenna and Radome, B.S.T.J., this issue, p. 1137.
6. Silver, S., *Microwave Antenna Theory and Design*, McGraw-Hill, New York, 1949, p. 192.
7. Lange, J., unpublished work.
8. Stratton, J. A., *Electromagnetic Theory*, McGraw-Hill, New York, 1941, p. 55.